Food Research International 131 (2020) 108988

Contents lists available at ScienceDirect

Food Research International

journal homepage: www.elsevier.com/locate/foodres

Dextrose equivalence of maltodextrins determines particle morphology development during single sessile droplet drying

I. Siemons[a], R.G.A. Politiek[a], R.M. Boom[a], R.G.M. van der Sman[b], M.A.I. Schutyser[a,*]

[a] Laboratory of Food Process Engineering, Wageningen University and Research, P.O. Box 17, 6700 AA Wageningen, the Netherlands
[b] Wageningen Food & Biobased Research, Wageningen University and Research, P.O. Box 17, 6700 AA Wageningen, the Netherlands

ARTICLE INFO

Keywords:
Single droplet drying
Morphology
Maltodextrins
Glass transition
Rheology

ABSTRACT

Particle morphology development during spray drying is critical to powder properties. The aim of this study was to investigate whether the dextrose equivalence (DE) of maltodextrins can be used as an indicator for the final particle morphology. Maltodextrins were characterized on glass transition temperature (T_g) and viscosity, where low DE-value maltodextrins exhibited higher T_g and viscosity than high DE maltodextrins (≥ 21). A new custom-built sessile single droplet dryer was used to analyse morphology development of minute maltodextrin droplets ($R_0 \sim 100$ μm) at 60 °C and 90 °C. Droplets with low DE showed early skin formation (2–5 s) and developed smoothly shaped particles with large cavities. Rheology on low DE maltodextrin films at dry matter of 82% (w/w) suggested that drying droplets acquired elasticity after locking providing resistance against surface compression. After locking morphology development is probably halted as the glassy state is approached. On the contrary, rheology on high DE maltodextrin (≥ 21) films at dry matter of 93% (w/w) suggested that drying droplets with high DE developed viscous skins, which are susceptible to surface deformations, leading to wrinkling, folding or creasing particle morphologies. The results demonstrated that DE-value may be used as an indicator for particle morphology development when interpreted in view of the process conditions.

1. Introduction

Drying of fluids, containing for example polymers and colloids, has gained great interest during the last decade (Both, Nuzzo et al., 2018; Fu, Woo, & Chen, 2012; Giorgiutti-Dauphiné & Pauchard, 2018; Lintingre, Lequeux, Talini, & Tsapis, 2016; Meng, Doi, & Ouyang, 2014; Sadek et al., 2015). Droplets of these fluids acquire different morphologies according to the material properties and conditions applied during formation. In turn the morphology affects the dried powder properties, including reconstitution behavior and flowability (Takeiti, Kieckbusch, & Collares-Queiroz, 2008; Walton & Mumford, 1999). Therefore, a sound understanding of morphology development during drying is necessary to control and steer final powder properties.

During spray drying, the solutes accumulate below the droplet's surface, due to rapid solvent evaporation. Eventually, this accumulation leads to the formation of a "skin" that has at least some characteristics of a solid (Pauchard & Allain, 2003; Vehring, 2008). The physico-chemical and mechanical characteristics of this skin significantly affect particle structure evolution towards its final morphology. Interactions of these aspects with drying conditions will result in morphological characteristics such as surface wrinkling and/or the formation of cavities. A closer study of these surface instabilities may be done via drying of single droplets under well-controlled and monitored conditions (Fu et al., 2012; Sadek, Schuck, Fallourd, & Jeantet, 2014; Schutyser, Both, Siemons, Vaessen, & Zhang, 2018). For example, Pauchard and Allain (2003a) studied buckling instabilities of colloidal particle suspensions and polymer solutions using sessile single droplet drying. They concluded that buckling requires a permeable, somewhat rigid skin which may still bend under the pressure of solvent evaporation. Sadek et al. (2014, 2015) studied wrinkling phenomena exploiting single droplet drying of colloidal casein suspensions. Droplet surface wrinkling was explained by the capacity of micelles to reduce their voluminosity as soft spheres in jamming conditions, resulting in a ductile elastic skin layer susceptible to surface distortion. Vacuole formation during drying of whey protein droplets was well described by Bouman et al. (2016) and Both, Karlina et al. (2018) and requires a rigid skin that resists bending, but still allows permeation of the solvent.

Physical effects responsible for the formation of different morphologies have been mostly studied with colloidal suspensions. Many spray-dried powders include carbohydrates, varying from simple sugars or disaccharides to polydisperse carbohydrate oligomers and polymers (Ubbink, Burbidge, & Mezzenga, 2008). Among the carbohydrates,

* Corresponding author.
E-mail address: maarten.schutyser@wur.nl (M.A.I. Schutyser).

https://doi.org/10.1016/j.foodres.2020.108988
Received 4 November 2019; Received in revised form 6 January 2020; Accepted 6 January 2020
Available online 08 January 2020

maltodextrins are particularly used in spray drying as drying aids and can serve as encapsulation agents for bioactive ingredients (Adhikari, Howes, Bhandari, & Troung, 2004; Renzetti, Voogt, Oliver, & Meinders, 2012). Typically, maltodextrins are obtained from starch polymers by acid hydrolysis, enzymatic hydrolysis, or a combination of both and are characterized by their dextrose equivalent (DE), being the fraction of hydrolyzed glucoside bonds (Loret, Meunier, Frith, & Fryer, 2004). Maltodextrins with different DE-values have different properties (Takeiti et al., 2008). Dokic et al. (1998), for instance showed a linear relation between viscosity and the DE-value of a maltodextrin. Others found a linear correlation between the DE-value and glass transition temperature (Avaltroni, Bouquerand, & Normand, 2004; Levine & Slade, 1986; Roos & Karel, 1991), which is in line with the well-known Fox-Flory equation (Fox & Flory, 1950).

In this specific study we investigate whether the DE of maltodextrins can also be used as an indicator for the final powder particle morphology. For this purpose, we investigated five different maltodextrins varying in DE. First, characteristics such as the molecular weight distributions, viscosities and glass transition temperatures as function of the maltodextrin concentration were measured. We hypothesize that especially the rheological characteristics at high concentrations can provide deeper insight in morphology development. Therefore, we also evaluated the mechanical properties of maltodextrins at high concentrations using thin film rheology on high dry matter thin films (Both, Tersteeg et al., 2019).

Morphology development during drying was analyzed using a new sessile single droplet drying system, where we make use of a piezo-electric dispenser capable of dispensing small droplets (~200 μm) at relatively high initial dry matter contents (30% (w/w)). We developed this system as most previously available sessile single droplet dryers relied on droplets larger than those relevant for spray drying. It is known that droplet size influences morphology development (Both, Siemons et al., 2019); therefore, we make use of a new system allowing the study of much smaller droplets, closer to the range of those in spray drying.

2. Materials and methods

2.1. Materials

All maltodextrins originate from corn-starch and were obtained from Roquette Frères (Lestrem, France). The following dextrose equivalents (DE) were used: DE5; DE12; DE21; DE29 and DE38. Solutions were prepared by adding the maltodextrins powders to demineralized water and stirring for at least 30 min until the solution was transparent. The final solutions had different dry matter concentrations depending on the experiment performed.

2.2. Molecular weight distribution

Molecular weight distributions of the different maltodextrins were determined by High Performance Liquid Chromatography (HPLC) using a Shodex KS-803 8.0 × 300 (mm) IDxLength + Guard column. The column is operated at 50 °C and connected to a refractive index (RI) detector (Shodex RI-501). Milli-Q water was used as eluent with a flow rate of 1 mL/min.

2.3. Glass transition temperature

Differential scanning calorimetry (DSC) experiments were performed to determine the glass transition temperature (T_g) of maltodextrins as function of their moisture content. The water content in powders was increased by a cold mixing procedure as described by Ruan et al. (1999), where a known amount of distilled water was frozen in liquid nitrogen in a mortar and the obtained ice crystals were ground into fine ice powder. Liquid nitrogen and appropriate amounts of maltodextrin powder were then added to the ice powder in the mortar and mixed by using the pestle. The mixture was stored at 4 °C for at least 24 h to ensure homogeneous distribution of the moisture before the DSC measurements.

The prepared samples (10–20 mg) were hermetically sealed in a DSC aluminum pan and introduced to a Pyris Diamond DSC (Perkin-Elmer, DSC 8000, Norwalk, USA). An empty pan was used as a reference. The pans were first equilibrated for 1 min at the lowest temperature of the selected DSC run (at least 30 °C below the expected T_g), after which a heating ramp followed with either 1 °C/min or 5 °C/min to the highest temperature (at least 30 °C above the expected T_g) of the DSC run to provide a good resolution of the transition. The pans were then equilibrated at the highest temperature of the selected run for 1 min and subsequently the sample was cooled at a rate of 10 °C/min to the lowest temperature of the selected run. The heating cycle was then repeated. The settings of the run were estimated based on the measured T_g values for different maltodextrins at varying moisture content as reported by Avaltroni et al. (2004) and Castro et al. (2016). Obtained DSC thermograms were analyzed using software interfaced with the DSC, and the T_g was determined from the onset point of the change in heat flow observed at the second heating ramp. All measurements were done in duplicate for each condition and the T_g values were averaged.

The experimental data were fitted with a combination of the Couchman-Karasz and Fox-Flory (Roos & Karel, 1991; Van Der Sman & Meinders, 2011). The Couchman-Karasz relation states:

$$T_g = \frac{y_w \Delta c_{P,w} T_{g,w} + y_s \Delta c_{p,s} T_{g,s}}{y_w \Delta c_{p,w} + y_s \Delta c_{p,s}} \tag{1}$$

Here y_i is the mass fraction ($i = w, s$ for water and solute), $T_{g,i}$ is the glass transition temperature for the pure component ($T_{g,w} = 139$ K), $\Delta c_{p,i}$is the change in the specific heat at the glass transition. For $\Delta c_{p,w}$ a value of 1.91 kJ/kg·K was used. The $\Delta c_{p,s}$ was considered similar for all maltodextrins at 0.426 kJ/ kg·K (Haene & Liederkerke, 1996; Van Der Sman & Meinders, 2011).

The glass transition of the anhydrous material, $T_{g,s}$, can be described by the Fox-Flory relation:

$$T_{g,s} = T_{g,s}^{\infty} - \frac{a_{FF}}{M} \tag{2}$$

$T_{g,s}^{\infty}$ (K) is the glass transition temperature for polymers with an infinite polymer chain length, a_{FF} (K·g/mol) is a constant and $M = 162 * \left(\frac{111.11}{DE}\right) + 18$ is the molecular weight of the polymer (Dokic et al., 1998). Combining the Couchman-Karasz and the Fox-Flory relations provides the following equation:

$$T_g = \frac{y_w \Delta c_{P,w} T_{g,w} + y_s \Delta c_{p,s} (T_{g,s}^{\infty} - \frac{a_{FF}}{M})}{y_w \Delta c_{p,w} + y_s \Delta c_{p,s}} \tag{3}$$

which simultaneously describes the effects of the water content and the molecular weight of the maltodextrin on the glass transition temperature. Equation (3) was fitted to the experimental data to obtain the $T_{g,s}^{\infty}$ and the a_{FF} parameters.

2.4. Rheology measurements

The rheological properties were investigated with a strain-controlled rheometer (MCR 502, Anton Paar). For viscosity measurements, solutions were first prepared at 20% (w/w) dry matter and subsequently concentrated using a rotational evaporator at 70 mBar at 50 °C as described by Both, Siemons et al. (2019). A shear rate sweep was performed using a concentric cup geometry (CC17, 16,660 mm × 24,858 mm (width × height), Anton Paar). The shear rate was logarithmically increased from 0.1 to 100 s^{-1}, with 15 measuring points with duration decreasing logarithmically from 300 to 1 s. Subsequently, the procedure was reversed, i.e. from 100 to 0.1 s^{-1} with 15 measurement points and logarithmically increasing duration of 1 to

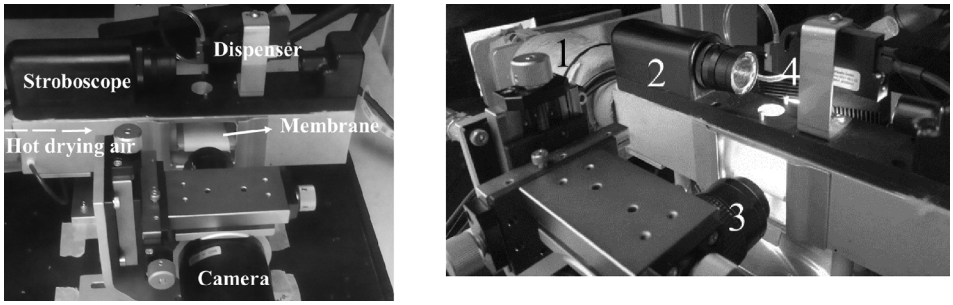

Fig. 1. Sessile single droplet drying setup. Left picture provides a front view of the setup. The right picture shows (1) the insulated air tunnel, (2) the stroboscope, (3) the camera, and (4) the PipeJet dispenser.

300 s. Samples of varying dry matter content were measured in duplicate; once including the reversed procedure, and once without the reversed procedure.

Amplitude and frequency sweeps were performed on thin films using a parallel-plate geometry at 50 °C as was described by Both, Tersteeg et al. (2019). Thin films were prepared with an initial dry matter of 30–60% (w/w), followed by an equilibration step in a climate chamber (Memmert, Germany) at 50 °C for three days (Table 1, Appendix A). Amplitude sweeps were performed to determine the extent of the linear viscoelastic regime. We tested a strain range of 0.1–100% at an angular frequency of 10 rad·s^{-1} with the normal force constant at 1 N. Frequency sweeps were subsequently performed at a shear strain of 0.05%. Data points (20) were collected over an angular frequency range of 0.01–100%. Measurements were done in duplicate or more.

2.5. Single droplet drying

Morphology development of maltodextrin solutions (30% (w/w) dry matter) during drying was studied using a novel sessile single droplet drying platform (Fig. 1). The droplet was dispensed by a PipeJet® NanoDispenser (BioFluidix, Germany) using 200-S PipeJet® Pipes (BioFluidix, Germany) on a hydrophobic membrane to retain the spherical shape (contact angle of the single droplet > 100°) of the droplet (PF3010 Polytetrafluoroethylene membrane, pore size 25–35 μm, porosity 55–60%, thickness 1 ± 0.25 mm) (Polyfluor Plastics BV, The Netherlands). The dispensing was controlled to obtain a desired droplet volume using BioFluidix Control Software V2.9 connected to a stroboscope (BioFluidix, Germany).

Droplets were dried in heated air (RH = 0%) at 60 °C or 90 °C and a flow velocity of 0.3 m/s using an insulated air feed tunnel as was originally designed by Perdana et al. (2011). Deposited droplets had an initial radius (R_0) of 100 μm ± 15 μm and were followed for a minimum of 20 s drying time w.r.t. their size and shape using a Monochrome USB 3.0 Camera (Edmund Optics, Germany) with a VZM™ 1000 Zoom Imaging Lens (Edmund Optics, Japan) at a frame rate of 35 fps. The obtained sequences were analyzed for the initial droplet size and locking points via image analysis using Image J software (National Institute of Health, USA). The locking point, which represents the onset of morphology development, was defined as the first visual observation of shape deviation of the drying sessile droplet during video analysis. At this point, the spherical shape of the droplet becomes distorted and shows first signs of cavity formation/denting. For all the formulations dried, experiments were performed at least in triplicate at both 60 °C and 90 °C. Thus, all image and data analyses correspond minimally to triplicates.

After drying, particles were studied using scanning electron microscopy (SEM). For SEM analysis, samples were fixed on the sample holder using carbon adhesive tabs. SEM images were taken at 5 kV, 3.74 pA, using a Phenom G2 Pure SEM (Thermo Fischer Scientific, The Netherlands). For all droplets a full image and a topographic image were made by a high sensitivity backscatter electron detector (Thermo Fischer Scientific, The Netherlands). Again, all analyses were performed in triplicate.

3. Results and discussion

3.1. Physicochemical properties

Higher DE-values have lower number average molecular weight (Rong, Sillick, & Gregson, 2009). However, low DE-value maltodextrins in particular, represent a blend of saccharides with a broad molecular weight distribution (Chronakis, 1998). The molecular weight distribution influences for example the viscosity and glass transition temperature, parameters relevant to drying behavior (Avaltroni et al., 2004; Castro et al., 2016). Therefore, we determined the molecular weight distribution of the maltodextrins (Fig. 2).

Maltodextrins DE5, DE12 and DE21 showed a broader distribution of molecular weights, with first elution peaks between 6 and 7 min and additional peaks after 8 min (Fig. 2). This broader distribution was also identified by Castro et al. (2016) for maltodextrins DE6, DE12, DE17 and DE19.

The first peaks in Fig. 2 for DE5, DE12 and DE21 correspond to higher molecular weight polymers. Maltodextrins DE5 and DE12 showed higher peaks around 6 to 7 min than maltodextrin DE21, indicating that they contained a larger fraction of high molecular weight polysaccharides. Maltodextrin DE21, however, consisted of a larger fraction low molecular weight oligo-saccharides than maltodextrins DE5 and DE12 as can be observed from the higher peaks after 8 min. Overall, the molecular weight distribution of the analyzed maltodextrins turned out to be narrower as DE-value increased, where maltodextrins DE29 and DE38 consisted mostly of low molecular

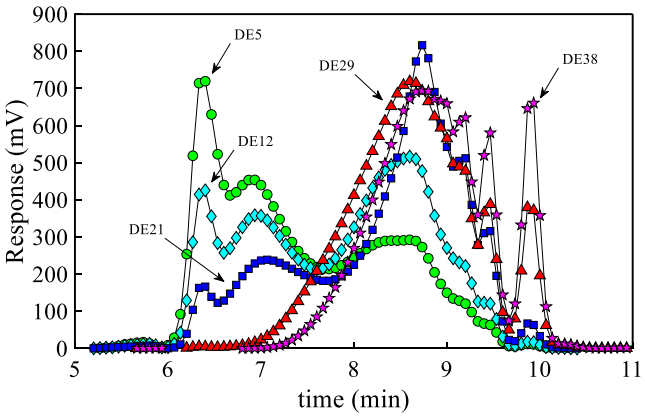

Fig. 2. Molecular weight distribution for maltodextrin DE5 (circles), DE12 (diamonds), DE21 (squares), DE29 (triangles) and DE38 (stars). Molecules with higher molecular weight elute first, followed by low molecular weight components.

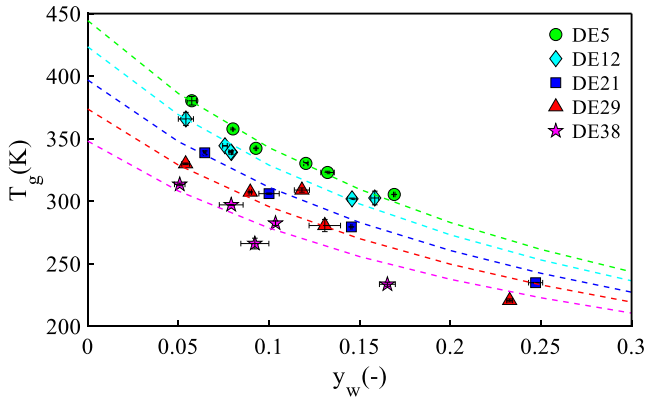

Fig. 3. Glass transition temperature (Tg) measured for maltodextrins as function of water content of the sample. Dotted lines are the model predictions (green: DE5, cyan: DE12, blue: DE21, red: DE29, magenta: DE38). (For interpretation of the references to colour in this figure legend, the reader is referred to the web version of this article.)

weight sugars.

In addition to the molecular weight distribution, glass transition temperatures and viscosities for the different maltodextrins were measured as function of water content (Figs. 3 and 4). The latter was done as these are critical physicochemical parameters characterizing the functionality and the structure of a matrix during the drying process (Avaltroni et al., 2004; Palzer, 2010). We first measured and modelled glass transition temperatures as function of water content for the different maltodextrins (Fig. 3). In agreement with literature, increasing glass transition temperatures were obtained for decreasing DE-values at a given dry matter content (Dokic et al., 1998). We fitted the measured glass transition temperatures by combining Couchman-Karasz and Fox-Flory (Eq. (3)), where all measured data points were included to estimate $T_{g,s}^{\infty}$ and a_{FF}. The optimum parameters $T_{g,s}^{\infty}$ and the constant a_{FF} were found to be 460 ± 5 K and $54.8 \cdot 10^3$ ± $0.41 \cdot 10^3$ K·g/mol, respectively. The values of $T_{g,s}^{\infty}$ and a_{FF} were close to literature values found: 450 K for fructans and 475 K for glucose-based polysaccharides (Van Der Sman, 2013) and $53 \cdot 10^3$ K·g/mol for various types of maltodextrins (Avaltroni et al., 2004). From Fig. 3 it can be observed that the fitted equation is in agreement with the experimental data. For maltodextrins DE29 and DE38, more deviations between theory and experiments can be observed as these contain higher amounts of glucoses (Van Der Sman & Meinders, 2011). This is related to the Fox-Flory equation, which more accurately describes glass transition for polymers at intermediate and high molecular weight (Novikov & Rössler, 2013; Van Der Sman & Meinders, 2011).

In addition, viscosity was measured as function of concentration (Fig. 4A). All the shear stress-shear rate flow curves indicated Newtonian behavior. From Fig. 4A it can be observed that maltodextrin DE5 had the highest viscosity upon concentration among the different DE samples, which was in line with our expectations based on the work of Avaltroni et al. (2004). Maltodextrins DE21, DE29 and DE38 showed quite similar viscosities upon concentration, which could be due to comparable molecular weight distributions (Fig. 2, Section 3.1).

Additionally, we plotted the viscosity of the samples as function of T_g/T as it was demonstrated already that viscosity of various carbohydrate solutions is governed by the ratio of T_g/T (Dupas-Langlet, Meunier, Pouzot, & Ubbink, 2019; van der Sman & Mauer, 2019; Van Der Sman & Meinders, 2013; Williams, Landel, & Ferry, 1955). T_g values were computed using the Fox-Flory and Couchman-Karasz equation (Eq. (3)). Fig. 4B suggests indeed that the viscosity of maltodextrin solutions scales with T_g/T, where a steeper increase in viscosity as function of T_g/T was obtained for low DE-value maltodextrins.

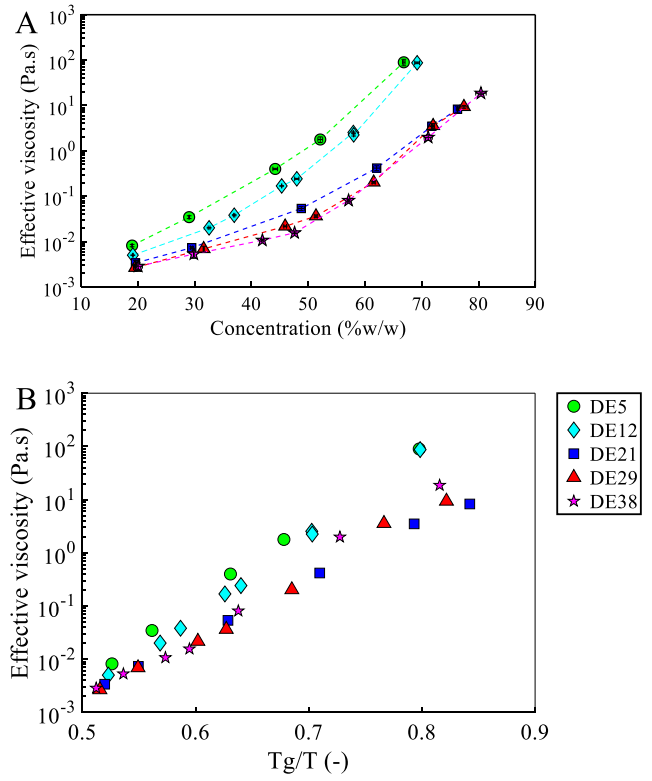

Fig. 4. (A) Viscosity of maltodextrins as function of concentration (% (w/w)). Dotted lines are drawn to guide the eye. (B) Viscosity as function of T_g/T (–). Viscosities are measured in duplicate at 20 °C. T_g was calculated by Equation (3) based on the moisture content of the sample.

3.2. Skin formation

Single droplets of maltodextrin solutions were dried at 60 °C and 90 °C to study the effect of DE-value on particle morphology development. Fig. 5 shows two time series of drying droplets as examples. An overview of all the time series collected at both drying air temperatures are presented in Figs. 11 and 12 in the Appendix A. Initially, a period of ideal drying was observed where mass transfer is externally limited and the droplet remains more or less spherical (Both, Karlina et al., 2018). In this first drying period, the evaporation rate was observed to be similar for all different DE-values (data not shown), which is in agreement with the findings of Both, Karlina et al. (2018). As the evaporation of water progresses, solutes accumulate at the droplet surface, resulting in a local increase of the viscosity near the droplet surface, which develops into a semi-solid thin layer referred to as a "skin". It is expected that all droplets eventually form a skin layer as the dimensionless Péclet number (ratio of the drying rate and the solute diffusivity in the droplet) quickly becomes > 1 during our drying experiments (Vehring, Foss, & Lechuga-Ballesteros, 2007). The critical concentration at which this skin starts to influence the drying process is sometimes called "locking point" and can be considered the onset of the development of the morphology (Both, Karlina et al., 2018; Tran, Avila-Acevedo, & Tsotsas, 2016).

We used the drop evolution images to analyze the relation between the locking points and the DE-value of the maltodextrins (Fig. 6A). Earlier locking points were obtained at higher drying air temperature as in agreement with Tran et al. (2016) and Both, Karlina et al. (2018) and explained by faster drying. Additionally, faster locking was observed for maltodextrin DE5 droplets than higher DE-value droplets dried at both drying air temperatures. This finding coincided with the observation that maltodextrin DE5 had the highest viscosity upon concentration among the different DE matrices (Fig. 4A), therefore it is likely that skin formation occurred earlier in the drying process. The normalized radius at the locking point as function of DE-value for both drying air

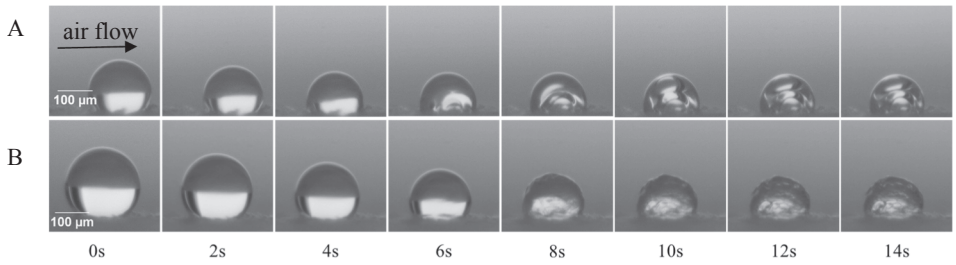

Fig. 5. Morphology developments in time for (A) maltodextrin DE5 and (B) maltodextrin DE38. The droplets were dried at 60 °C and the air flow (0.3 m/s) came from the left side as indicated by the arrow.

temperatures is provided in Fig. 6B. A larger normalized radius was obtained at the locking point for lower DE-values (Fig. 6B). Faster locking at larger normalized radius for low DE-value droplets is supported by the work of Sugiyama et al. (2006), where it was observed that single droplets of high molecular weight components deformed earlier in the drying process, while they were still large, as opposed to droplets of low molecular weight components that deformed later during drying when they were smaller. It should be noted from Fig. 6A and B that the drying air temperature influenced the locking point time, however, it did not affect the normalized radius at the start of morphology development; the relative size of the droplet at the onset of morphology development is temperature independent. This finding is in agreement with the work of Lin and Chen (2004), where they demonstrated that the drying air temperature had only little effect on the droplet diameter change during drying of 30% (w/w) initial solids droplets.

3.3. Mechanical properties of maltodextrins at high concentrations

From the locking point on, different particle structures develop, which is greatly affected by the stability of the skin formed (Both, Tersteeg et al., 2019; Pauchard & Allain, 2003b; Sadek et al., 2015). According to Pauchard and Allain (2003a), skin stability is determined by both mechanical characteristics and by physicochemical properties of the system and their according time and space dependencies. Both, Tersteeg et al. (2019) demonstrated that oscillatory frequency sweep tests on equilibrated thin films at high dry matter concentrations can provide information on the resistance against deformation of the material studied. This information can then be linked to deformation of the droplets during drying. Therefore, we prepared partially dried thin films (≥82% (w/w) dry matter) and measured the frequency dependence of the loss and storage modulus in the frequency range of 0.1–100 rad/s (Fig. 7).

In Fig. 7A we compare the rheological response of thin maltodextrin DE5 and DE12 films at dry matter of 82% (w/w). At 82% (w/w) dry matter, maltodextrin DE12 films exhibit typical features of viscoelastic behavior of polymers (Sperling, 2001; Sunthar, 2012). At low frequency the response was viscous and followed by a cross-over to a broad plateau region. This plateau region, where G' dominates over G'', is typically associated with rubbery material and was already observed by Both, Tersteeg et al. (2019). For maltodextrin DE5 at 82% (w/w), G'' dominates of G' in the entire range of frequencies investigated, which implies viscous behavior for DE5 at this dry matter. However, based on the rheological response of DE12, the molecular weight distribution (Fig. 2), the higher T_g and accordingly higher viscosity values found for maltodextrin DE5 (Figs. 3 and 4), we hypothesize that maltodextrin DE5 at this dry matter is in a transition region towards glassy behavior. This was confirmed when we prepared thin maltodextrin DE5 films at dry matter content 90% (w/w). These films showed cracks on the surface, consistent with glass behavior (Gianfrancesco, Vuataz, Mesnier, & Meunier, 2012). Beyond the angular frequencies measured here, G' will again dominate G″ as the maltodextrins are virtually immobile and thus exhibit glassy behavior.

For the lower molecular weight maltodextrins DE21, DE29 and DE38, we were able to prepare thin films at a dry matter content of 93% (w/w). These films did not exhibit a rubbery region as the smaller sugar molecules cannot entangle. Fig. 7B shows viscous behavior for the thin films of DE21, 29 and 38 at dry matter of 93% (w/w). These high value DE maltodextrins will likely exhibit only glassy behavior at even higher dry matter contents (≥93% (w/w)).

3.4. Final particle morphologies

An overview of the final morphologies as obtained after single droplet drying at both drying air temperatures is provided in a morphology diagram (Fig. 8). Generally, low DE-values resulted in smoothly shaped particles with large cavities, whereas higher DE-values showed more surface irregularities during drying and ultimately wrinkled particle morphologies could be observed. Maltodextrin DE5 at drying air temperatures of 60 °C and 90 °C and maltodextrin DE12 at 60 °C formed smooth particles with large internal cavities and little or no surface distortions. These hollow particles with smooth surfaces

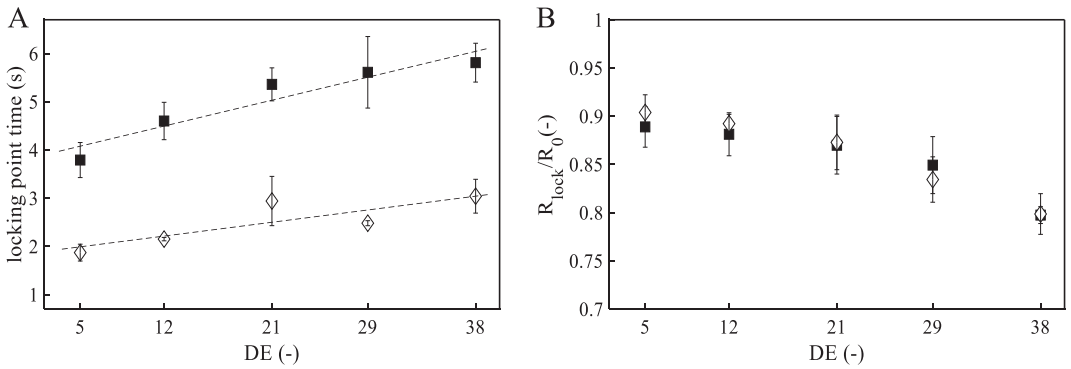

Fig. 6. Droplets were dried at 60 °C (squares) and 90 °C (diamonds) (A) Locking point time as function of DE-value. Dotted lines are drawn to guide the eye. (B) Normalized radius (R_{lock}/R_0) at the locking point of the droplets as function of DE-value.

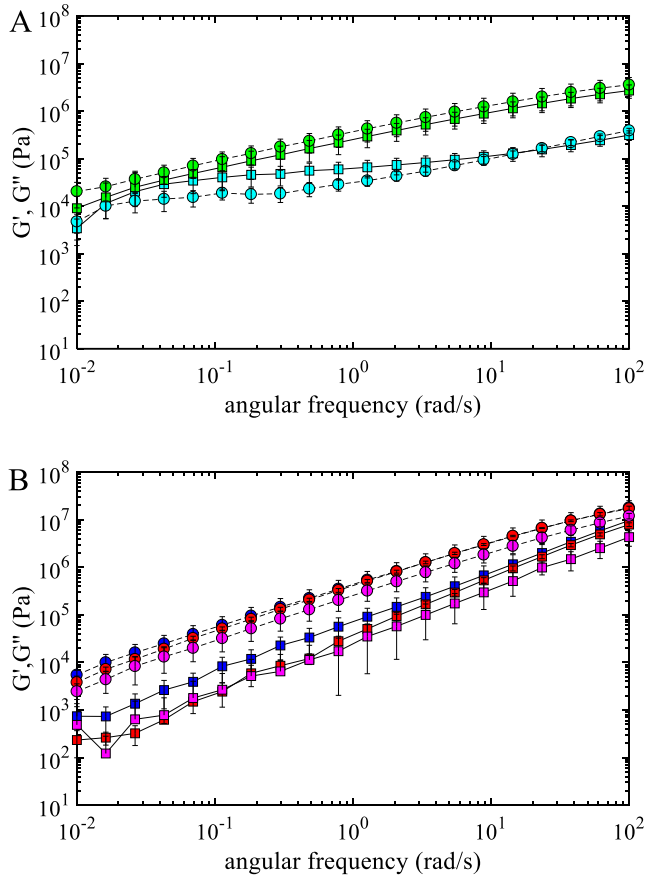

Fig. 7. Storage and loss moduli (squares and circles, respectively) as a function of the angular frequency for (A) maltodextrins DE5 and DE12 (green: DE5, cyan: DE12) measured at 82% (w/w) dry matter, 0.54 mm thick; (B) maltodextrins DE21, DE29 and DE38 (blue: DE21, red: DE29, magenta: DE38) at 93% (w/w), 0.62 mm thick. (For interpretation of the references to colour in this figure legend, the reader is referred to the web version of this article.)

were also observed after single droplet drying of unhydrolyzed starch solutions with 30% (w/w) initial dry matter at 80 °C and 140 °C (Adhikari, Howes, Bhandari, & Truong, 2000). Maltodextrin DE12 showed a transition from a smooth surface after drying at 60 °C to a more dented structure after drying at 90 °C; hence, DE12 was just in between two regimes. A similar dented structure was previously observed by Both, Nuzzo et al. (2018) for sessile single droplet drying of maltodextrin DE12 at 90 °C (R_0 of ~550 μm). Dented morphologies were also observed for maltodextrins DE21, DE29 and DE38 at both drying air temperatures. Maltodextrins DE21 and DE29 showed very similar denting patterns; yet, for DE29 coarser edges were observed using scanning electron microscopy (Fig. 8 SEM column). Maltodextrin DE38 had a smoother and more furrowed pattern, with sometimes a few large indentations.

From locking onward, the temperature of the droplet will increase as shown in Fig. 9 (Ziaee et al., 2019). After locking, the temperature will gradually converge to the drying air temperature. We suspect that at this time, the skin stability will dictate the final morphology developed. If then the droplet temperature is in close proximity to its surface glass transition temperature, molecular motions are largely restricted to short-range rotational motions and vibrations, and droplet skins have adequate mechanical strength to resist most mechanical surface stresses developed during drying. Here, we expect that the morphology development is halted. These expectations are to some extent in line with the work of Werner et al. (2008), who concluded that mechanical stresses developed in droplet skins are related to the proximity of the surface to its glass transition.

3.4.1. Low DE-value maltodextrins

The maltodextrins DE5 and DE12 dried at both drying air temperatures, developed a skin at an earlier stage than droplets with higher DE maltodextrins, which was explained by the steeper increase in viscosities upon concentration (Section 3.1). After locking, these droplets remained fairly spherical and developed large cavities (Appendix A, Figs. 11 and 12). The smooth particles obtained after drying, suggest that for these droplets a critical skin stability is reached relatively early in the drying process, close to the locking point. These stable skins cannot deform on the timescales of the drying process and thus can withstand the internal stresses that are developed during drying. The spherical form of the droplet is therefore retained, and buckling instabilities are almost lacking (Giorgiutti-Dauphiné & Pauchard, 2018).

We suspect that this smooth and hollow morphology may be explained by the acquired skin elasticity soon after locking, resulting in skins that are more stable against surface stressed developed. The acquired elasticity can be confirmed by the observation of a broad rubbery plateau region for DE12 thin films at 82% (w/w) dry matter (Fig. 7A). Maltodextrin DE5 probably develop elastic skins earlier in the drying process than DE12, which is in agreement with Fig. 7A. The elasticity likely results from physical entanglement ($c > c^*$) due to the large fraction high molecular weight polysaccharides present, but there is also a chance it might result from retrogradation at lower temperatures (Sobolewska-Zielińska & Fortuna, 2010; Sperling, 2001). This elastic skin still allows for water evaporation, which makes the maltodextrin DE5 and DE12 droplets amenable to the formation of cavities. As water evaporates, the elastic skin is compressed, resulting in an increase in the elastic energy of deformation, which is reduced again by the formation of a cavity (Meng et al., 2014). Ultimately, the elastic skin approaches the glassy state, which happens earlier for maltodextrin DE5 droplets than DE12 droplets (Fig. 3).

It should be noted that maltodextrin DE12 droplets dried at 90 °C resulted in dented particles. The latter could be the consequence of a delayed glass transition; a higher drying air temperature could have resulted in an increase in the droplet temperature, consequently postponing transition to the glassy state. Therefore, it could be that DE12 skins at 90 °C exhibit rubbery behavior for a longer drying time as compared to DE5 at 60 °C and 90 °C, and DE12 at 60 °C, possibly resulting in more surface instabilities. Thus, faster transition from elastic/rubbery to glassy skins may even further decrease the surface instabilities observed after drying.

3.4.2. High DE-value maltodextrins

Maltodextrins consisting of short oligomers and small sugars do not develop any form of elasticity shortly after locking. These droplets increase slowly in viscosity upon concentration, and after locking their skins will not be sufficiently stable to withstand stresses exerted on the droplet surface, leading to deformation of the surface. The latter was confirmed by thin film rheology, where at a dry matter content of 93% (w/w), films with maltodextrin DE21, DE29 and DE38 still exhibited viscous behavior (Fig. 7B). Most likely, skin stability is only obtained when the droplet surface approaches the glassy state (Fig. 9).

The final morphologies obtained here for maltodextrins with higher DE-values are well in line with the work of Li et al. (2011), who investigated surface wrinkling patterns on a core-shell soft sphere. Li et al. (2012) found that the morphological instability of a soft material can be divided into three distinct phenotypes: wrinkling, folding and creasing. Initially, during early stage of drying the sphere shrinks isotropically. During drying, the shrinkage of the soft sphere exceeds a critical value and the sphere will buckle and form a regular pattern of pentagons and hexagons to release the circumferential compression within the shell. This pattern is comparable to the final morphologies we here observe with maltodextrin DE12 at 90 °C and maltodextrin DE21 at 60 °C.

With further shrinking of the droplet, the phenotype changes from a wrinkling pattern to a folding pattern as some of the polygons merge with their neighbors, while others form troughs; such a pattern may be

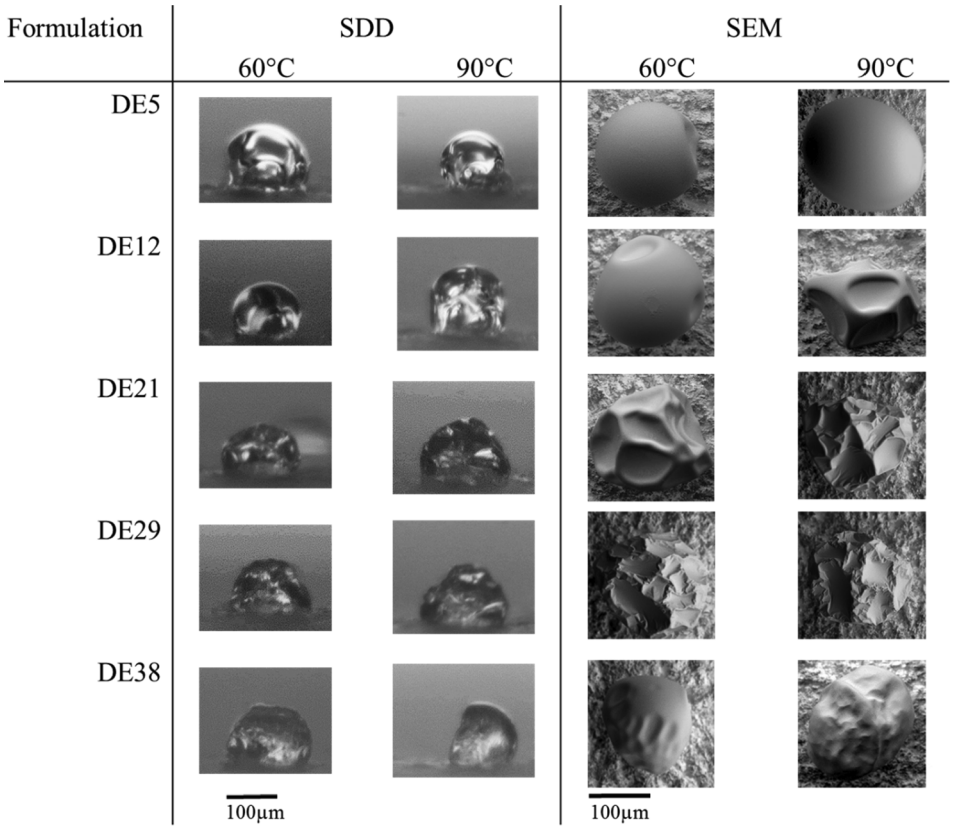

Fig. 8. Final particle morphologies for the different maltodextrins when dried at 60 °C and 90 °C with a velocity of 0.3 m/s for droplets with $R_0 = 100 \pm 15$ μm. Column named SDD shows the morphologies collected by the camera of the single droplet drying setup. Column SEM shows the scanning electron images of dried particles, note that these images are not necessarily the same droplets as shown in the SDD column. Scale bars are provided for the separate columns.

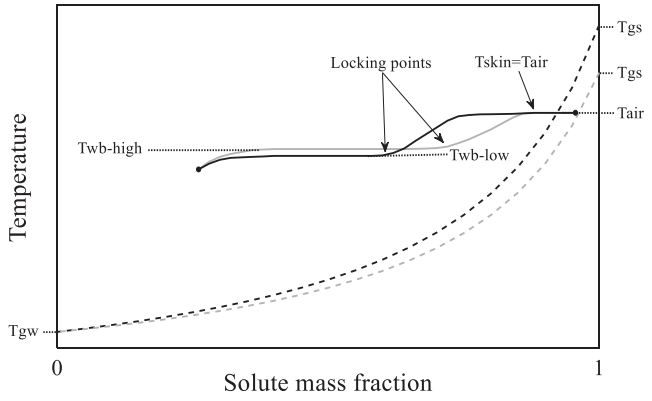

Fig. 9. Schematic diagram showing the droplet temperature (Low DE: black solid line and high DE: grey solid line) during single droplet drying. Glass transition curves of the skin as function of solute mass fraction are drawn (Low DE: black dashed line, high DE: grey dashed line). When the droplet skin temperature is in close proximity to its surface glass transition temperature, morphology development is halted. Tgw and Tgs are the glass transition temperatures of the water and dry solute, respectively. Wet bulb temperature (Low DE: Twb-low and high DE: Twb-high) and temperature of the drying air (Tair) are indicated. Droplet temperature profiles differ for low and high DE maltodextrins as assumed based on locking point analysis and sorption isotherms (Van Der Sman & Meinders, 2011).

related to the morphologies obtained with maltodextrin DE21 at 90 °C and maltodextrin DE29 at 60 and 90 °C. When the troughs that are formed deepen and the ridges become sharper, eventually a labyrinthine topography is formed, which resembles the final morphologies that we obtained with maltodextrin DE38 at 90 °C. This type of morphology could be referred to as “creasing”, which is formed when an initial soft and smooth surface forms ridges or sulci.

4. Conclusions

Particle morphology development during spray drying is critical to the final powder properties. Maltodextrins are frequently spray-dried and can develop both a hollow sphere morphology and a wrinkled or creased morphology. Here we have investigated whether the dextrose equivalence (DE) of maltodextrins can be used as an indicator for the final powder particle morphology. To investigate this in detail, we employed a newly designed sessile single droplet dryer.

Low DE maltodextrins (≤ 12) are only slightly hydrolysed and have a broad molecular weight distribution. They exhibit higher glass transition temperatures and viscosities than high DE maltodextrins (≥ 21) consisting mostly of oligosaccharides. We showed that the viscosity of maltodextrins can be described by the ratio of glass transition temperature to the system temperature Tg/T.

Morphology development with solutions of low DE maltodextrins starts relatively early in the drying process. We hypothesize that the skins of droplets with low DE maltodextrins show significant elasticity after locking. Thus, these are able to withstand surface compression, leading to smooth particles having cavities. These low DE-value maltodextrin skins approach the glassy state slightly later, halting morphology development. In contrast, high DE droplet skins do not develop significant elasticity after locking and these skins become mostly viscous, allowing deformation due to surface compression, leading to wrinkling, folding or creasing, depending on the viscosity during deformation.

Our results demonstrate that the DE-value is an indicator for the particle morphology, when it is interpreted in the context of process conditions. There is a direct link between the rheological properties at high concentrations and morphology development of powder particles. In the future, it would be worthwhile to further investigate the rheology of maltodextrins in vicinity of the glass transition temperature. This will eventually allow better prediction of the morphology, which can then be used to predict powder properties such as flowability and rehydration behaviour. Key results of our study are summarized in Fig. 10.

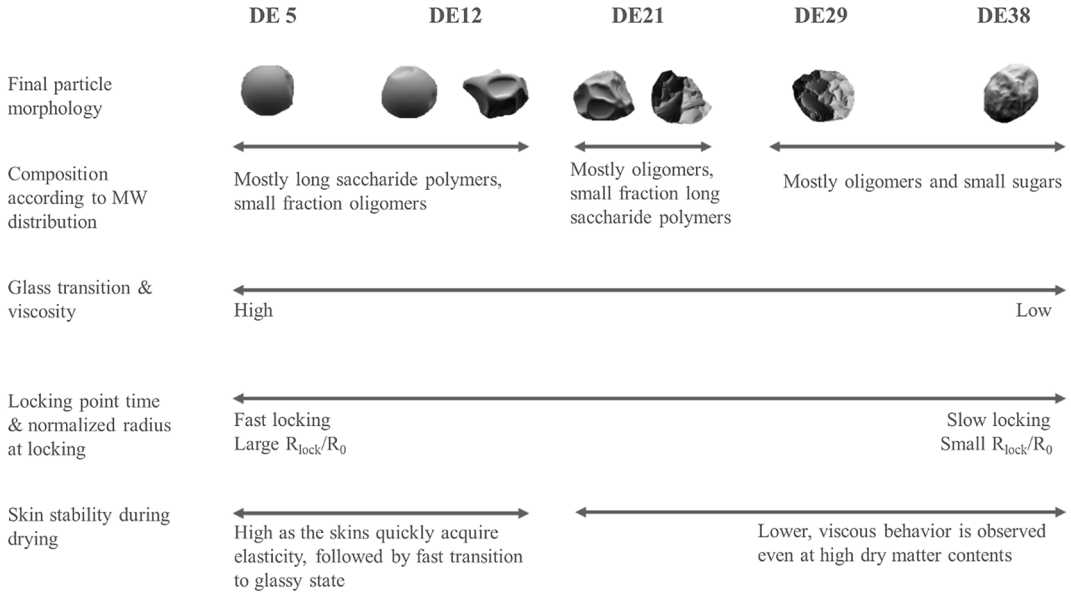

Fig. 10. Summary of results relating to the final particle morphologies.

CRediT authorship contribution statement

I. Siemons: Conceptualization, Methodology, Validation, Formal analysis, Investigation, Writing - original draft. **R.G.A. Politiek:** Methodology, Validation, Investigation. **R.M. Boom:** Writing - original draft, Supervision. **R.G.M. van der Sman:** Conceptualization, Methodology, Writing - original draft. **M.A.I. Schutyser:** Conceptualization, Methodology, Writing - original draft, Funding acquisition.

Declaration of Competing Interest

The authors declared that there is no conflict of interest.

Acknowledgements

This research is supported by the Netherlands Organization for Scientific Research (NWO) (grant number 15459). The authors would like to thank the user committee for stimulating discussions on morphology development. Furthermore, we would like to thank Eline Verbaanderd-Both for her contribution to this work.

Appendix A

See Table 1, Figs. 11 and 12.

Table 1
Thin films for rheology measurements were prepared by partial drying of the solutions in an oven set at 80 °C, followed by an equilibration step in a climate chamber. Sample volumes, oven times and relative humidity (RH) of the climate chamber are indicated. NA indicates no partial drying in an oven was required before equilibration in the climate chamber. Average dry matter contents and thickness are provided.

	Sample preparation			Sample properties	
DE	Volume (mL)	Oven time (min)	RH (%)	D.M. % (w/w)	Thickness (mm)
5	6	115	82–85	82 ± 0.5	0.62 ± 0.11
12	6–7	115	85	82 ± 0.3	0.45 ± 0.01
21	4.5–5	NA	65	93 ± 0.5	0.62 ± 0.05
29	5	NA	55	94 ± 0.2	0.61 ± 0.04
38	5	NA	50	93 ± 0.3	0.65 ± 0.04

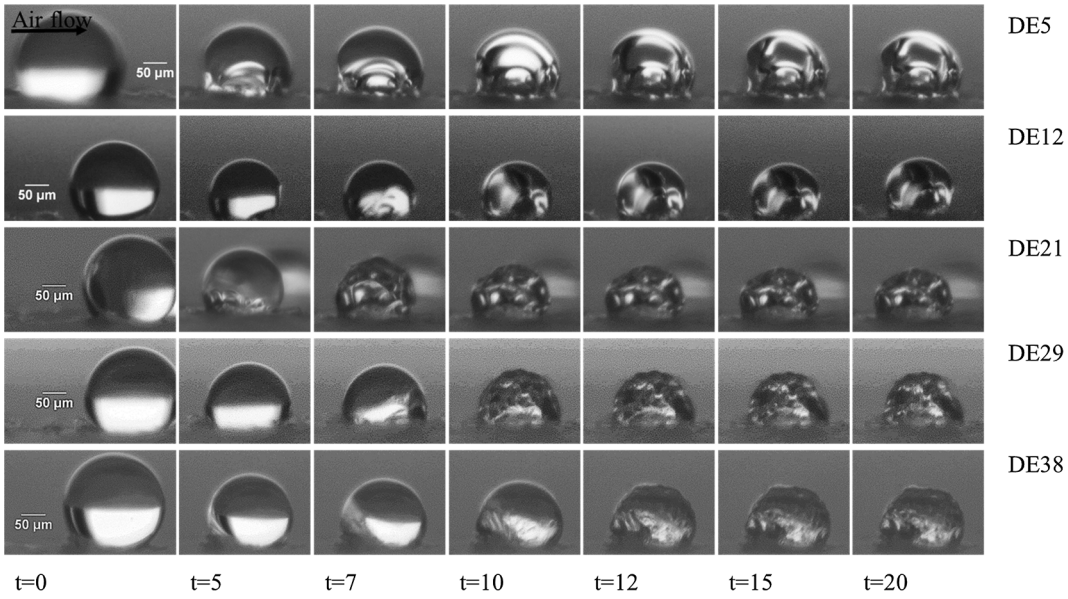

Fig. 11. Morphology development in time (s) for maltodextrins dried at 60 °C. The air flow (0.3 m/s) came from the left side as indicated by the arrow. R_0 = 100 ± 15 µm.

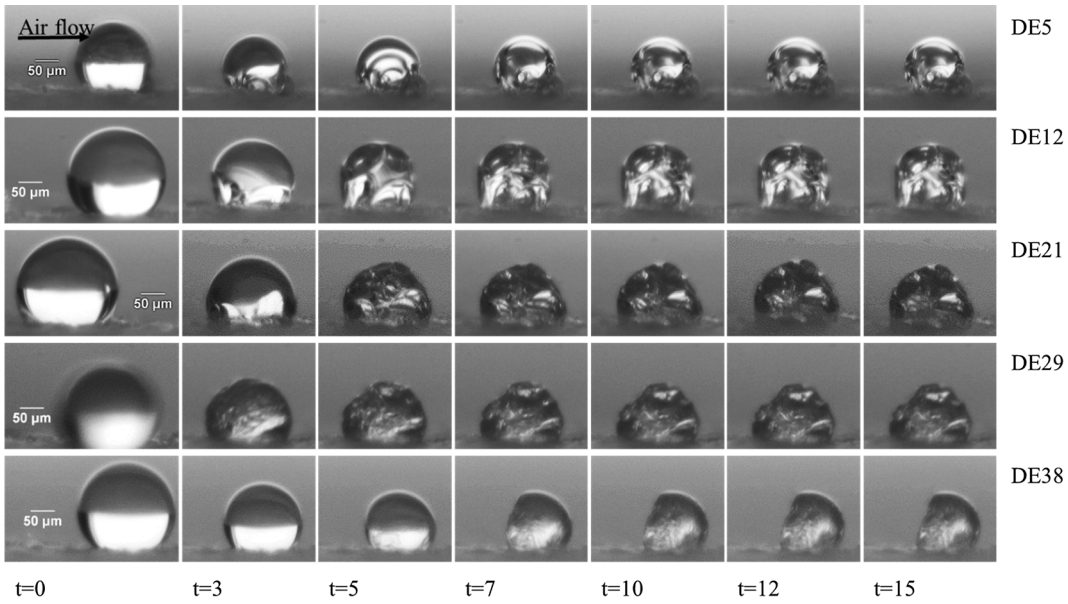

Fig. 12. Morphology development in time (s) for maltodextrins dried at 90 °C. The air flow (0.3 m/s) came from the left side as indicated by the arrow. R_0 = 100 ± 15 µm.

Appendix B. Supplementary material

Supplementary data to this article can be found online at https://doi.org/10.1016/j.foodres.2020.108988.

References

Adhikari, B., Howes, T., Bhandari, B. R., & Truong, V. (2000). Experimental studies and kinetics of single drop drying and their relevance in drying of sugar-rich foods: A review. *International Journal of Food Properties, 3*(3), 323–351.

Adhikari, B., Howes, T., Bhandari, B. R., & Troung, V. (2004). Effect of addition of maltodextrin on drying kinetics and stickiness of sugar and acid-rich foods during convective drying: Experiments and modelling. *Journal of Food Engineering, 62*(1), 53–68.

Avaltroni, F., Bouquerand, P. E., & Normand, V. (2004). Maltodextrin molecular weight distribution influence on the glass transition temperature and viscosity in aqueous solutions. *Carbohydrate Polymers, 58*(3), 323–334.

Both, E. M., Karlina, A. M., Boom, R. M., & Schutyser, M. A. I. (2018a). Morphology development during sessile single droplet drying of mixed maltodextrin and whey protein solutions. *Food Hydrocolloids, 75*, 202–210.

Both, E. M., Nuzzo, M., Millqvist-Fureby, A., Boom, R. M., & Schutyser, M. A. I. (2018b). Morphology development during single droplet drying of mixed component formulations and milk. *Food Research International, 109*(April), 448–454.

Both, E. M., Siemons, I., Boom, R. M., & Schutyser, M. A. I. (2019a). The role of viscosity in morphology development during single droplet drying. *Food Hydrocolloids, 94*, 510–518.

Both, E. M., Tersteeg, S. M. B., Boom, R. M., & Schutyser, M. A. I. (2019b). Drying kinetics and viscoelastic properties of concentrated thin films as a model system for spray

drying. *Colloids and Surfaces A: Physicochemical and Engineering Aspects, 585*.
Bouman, J., Venema, P., de Vries, R. J., van der Linden, E., & Schutyser, M. A. I. (2016). Vacuole and hole formation during drying of sessile whey protein droplets. *Food Research*.
Castro, N., Durrieu, V., Raynaud, C., & Rouilly, A. (2016). Influence of DE-value on the physicochemical properties of maltodextrin for melt extrusion processes. *Carbohydrate Polymers, 144*, 464–473.
Chronakis, I. S. (1998). On the molecular characteristics, compositional properties, and structural-functional mechanisms of maltodextrins: A review. *Critical Reviews in Food Science and Nutrition, 38*(7), 599–637.
Dokic, P., Jakovljevic, J., & Dokic-Baucal, L. (1998). Molecular characteristics of maltodextrins and rheological behaviour of diluted and concentrated solutions. *Colloids and Surfaces A: Physicochemical and Engineering Aspects, 141*(3), 435–440.
Dupas-Langlet, M., Meunier, V., Pouzot, M., & Ubbink, J. (2019). Influence of blend ratio and water content on the rheology and fragility of maltopolymer/maltose blends. *Carbohydrate Polymers, 213*(November 2018), 147–158.
Fox, T. G., & Flory, P. J. (1950). Second order transition temperature and related properties of PS. *Journal of Applied Physics, 21*(6), 581–591.
Fu, N., Woo, M. W., & Chen, X. D. (2012a). Single droplet drying technique to study drying kinetics measurement and particle functionality: A review. *Drying Technology, 30*(February 2015), 1771–1785.
Fu, N., Woo, M. W., Chen, X. D., Fu, N., Woo, M. W., & Chen, X. D. (2012b). Single droplet drying technique to study drying kinetics measurement and particle functionality: A review. *Drying Technology, 30*(February 2015), 1771–1785.
Gianfrancesco, A., Vuataz, G., Mesnier, X., & Meunier, V. (2012). New methods to assess water diffusion in amorphous matrices during storage and drying. *Food Chemistry, 132*(4), 1664–1670.
Giorgiutti-Dauphiné, F., & Pauchard, L. (2018). Drying drops: Drying drops containing solutes: From hydrodynamical to mechanical instabilities. *European Physical Journal E, 41*(3).
D'Haene, P., & Van Liederkerke, B. (1996). Viscosity prediction of starch hydrolysates from single point measurements. *Starch-Stärke, 48*(9), 327–334.
Levine, H., & Slade, L. (1986). A polymer physico-chemical approach to the study of commercial starch hydrolysis products (SHPs). *Carbohydrate Polymers, 6*(3), 213–244.
Li, B., Cao, Y. P., Feng, X. Q., & Gao, H. (2012). Mechanics of morphological instabilities and surface wrinkling in soft materials: A review. *Soft Matter, 8*(21), 5728–5745.
Li, B., Jia, F., Cao, Y. P., Feng, X. Q., & Gao, H. (2011). Surface wrinkling patterns on a core-shell soft sphere. *Physical Review Letters, 106*(23), 2–5.
Lin, S. X. Q., & Chen, X. D. (2004). Changes in milk droplet diameter during drying under constant drying conditions investigated using the glass-filament method. *Food and Bioproducts Processing, 82*(3), 213–218.
Lintingre, E., Lequeux, F., Talini, L., & Tsapis, N. (2016). Control of particle morphology in the spray drying of colloidal suspensions. *Soft Matter, 12*(36), 7435–7444.
Loret, C., Meunier, V., Frith, W. J., & Fryer, P. J. (2004). Rheological characterisation of the gelation behaviour of maltodextrin aqueous solutions. *Carbohydrate Polymers, 57*(2), 153–163.
Meng, F., Doi, M., & Ouyang, Z. (2014). Cavitation in drying droplets of soft matter solutions. *Physical Review Letters, 113*(9), 1–5.
Novikov, V. N., & Rössler, E. A. (2013). Correlation between glass transition temperature and molecular mass in non-polymeric and polymer glass formers. *Polymer, 54*(26), 6987–6991.
Palzer, S. (2010). The relation between material properties and supra-molecular structure of water-soluble food solids. *Trends in Food Science and Technology, 21*(1), 12–25.
Pauchard, L., & Allain, C. (2003a). Mechanical instability induced by complex liquid desiccation. *Comptes Rendus Physique, 4*(2), 231–239.
Pauchard, L., & Allain, C. (2003b). Stable and unstable surface evolution during the drying of a polymer solution drop. *Physical Review E – Statistical Physics, Plasmas, Fluids, and Related Interdisciplinary Topics, 68*(5), 1–4.
Perdana, J., Fox, M. B., Schutyser, M. A. I., & Boom, R. M. (2011). Single-droplet experimentation on spray drying: Evaporation of a sessile droplet. *Chemical Engineering and Technology, 34*(7), 1151–1158.
Renzetti, S., Voogt, J. A., Oliver, L., & Meinders, M. B. J. (2012). Water migration mechanisms in amorphous powder material and related agglomeration propensity. *Journal of Food Engineering, 110*(2), 160–168.
Rong, Y., Sillick, M., & Gregson, C. M. (2009). Determination of dextrose equivalent value and number average molecular weight of maltodextrin by osmometry. *Journal of Food Science, 74*(1), 33–40.
Roos, Y. H., & Karel, M. (1991). Phase transitions of mixtures of amorphous polysaccharides and sugars. *Biotechnology Progress, 7*(1), 49–53.
Ruan, R., Long, Z., Chen, P., Huang, V., Almaer, S., & Taub, I. (1999). Pulse NMR study of glass transition in maltodextrin. *Journal of Food Science, 64*(1), 6–9.
Sadek, C., Schuck, P., Fallourd, Y., Pradeau, N., Le Floch-Fouere, C., & Jeantet, R. (2015). Drying of a single droplet to investigate process–structure–function relationships: A review. *Dairy Science & Technology, 95*(6), 771–794.
Sadek, C., Li, H., Schuck, P., Fallourd, Y., Pradeau, N., Le Floch-Fouéré, C., & Jeantet, R. (2014). To what extent do whey and casein micelle proteins influence the morphology and properties of the resulting powder? *Drying Technology, 32*(13), 1540–1551.
Sadek, C., Pauchard, L., Schuck, P., Fallourd, Y., Pradeau, N., Le Floch-Fouéré, C., & Jeantet, R. (2015). Mechanical properties of milk protein skin layers after drying: Understanding the mechanisms of particle formation from whey protein isolate and native phosphocaseinate. *Food Hydrocolloids, 48*, 8–16.
Schutyser, M. A. I., Both, E. M., Siemons, I., Vaessen, E. M. J., & Zhang, L. (2018). Gaining insight on spray drying behavior of foods via single droplet drying analyses. *Drying Technology*, 1–10.
Sobolewska-Zielińska, J., & Fortuna, T. (2010). Retrogradation of starches and maltodextrins of origin various. *Acta Scientiarum Polonorum, Technologia Alimentaria, 9*(1), 71–81.
Sperling, L. H. (2001). *Introduction to physical polymer science* (3rd ed.). John Wiley Sons Ltd.
Sugiyama, Y., Larsen, R. J., Kim, J. W., & Weitz, D. A. (2006). Buckling and crumpling of drying droplets of colloid-polymer suspensions. *Langmuir, 22*(14), 6024–6030.
Sunthar, P. (2012). Polymer Rheology. *Robust Process Development and Scientific Molding*, 27–41. https://doi.org/10.3139/9783446433427.003.
Takeiti, C. Y., Kieckbusch, T. G., & Collares-Queiroz, F. P. (2008). Morphological and physicochemical characterization of commercial maltodextrins with different degrees of dextrose-equivalent. *International Journal of Food Properties, 13*(2), 411–425.
Tran, T. T. H., Avila-Acevedo, J. G., & Tsotsas, E. (2016). Enhanced methods for experimental investigation of single droplet drying kinetics and application to lactose/water. *Drying Technology, 34*(10), 1185–1195.
Ubbink, J., Burbidge, A., & Mezzenga, R. (2008). Food structure and functionality: A soft matter perspective. *Soft Matter, 4*(8), 1569–1581.
Van Der Sman, R. G. M. (2013). Predictions of glass transition temperature for hydrogen bonding biomaterials. *Journal of Physical Chemistry B, 117*(50), 16303–16313.
van der Sman, R. G. M., & Mauer, L. J. (2019). Starch gelatinization temperature in sugar and polyol solutions explained by hydrogen bond density. *Food Hydrocolloids, 94*(March), 371–380.
Van Der Sman, R. G. M., & Meinders, M. B. J. (2011). Prediction of the state diagram of starch water mixtures using the Flory-Huggins free volume theory. *Soft Matter, 7*(2), 429–442.
Van Der Sman, R. G. M., & Meinders, M. B. J. (2013). Moisture diffusivity in food materials. *Food Chemistry, 138*(2–3), 1265–1274.
Vehring, R. (2008). Pharmaceutical particle engineering via spray drying. *Pharmaceutical Research, 25*(5), 999–1022.
Vehring, R., Foss, W. R., & Lechuga-Ballesteros, D. (2007). Particle formation in spray drying. *Journal of Aerosol Science, 38*(7), 728–746.
Walton, D. E., & Mumford, C. J. (1999). Spray dried products – Characterization of particle morphology. *Trans IChemE, 77*(January), 21–38.
Werner, S. R. L., Edmonds, R. L., Jones, J. R., Bronlund, J. E., & Paterson, A. H. J. (2008). Single droplet drying: Transition from the effective diffusion model to a modified receding interface model. *Powder Technology, 179*(3), 184–189.
Williams, M. L., Landel, R. F., & Ferry, J. D. (1955). The temperature dependence of relaxation mechanisms in amorphous polymers and other glass-forming liquids. *Journal of the American Chemical Society, 77*(14), 3701–3707.
Ziaee, A., Albadarin, A. B., Padrela, L., Femmer, T., O'Reilly, E., & Walker, G. (2019). Spray drying of pharmaceuticals and biopharmaceuticals: Critical parameters and experimental process optimization approaches. *European Journal of Pharmaceutical Sciences, 127*(November), 300–318.